Check for updates

CO + NH₃ coupling denitration at low temperatures over manganese/activated carbon catalysts

Liubin Luo, [ID] ab Bangfu Huang,*ab Zhe Shi,ab Zhenjing Wen, [ID] ab Wanjun Li,ab Gaoyong Zi [ID] ab and Linjing Yanga

To explore the mechanism of low-temperature carbon monoxide and ammonia (CO + NH₃) coupling denitration of manganese/activated carbon (Mn/AC) catalysts, Mn/AC series catalysts were prepared using the impregnation method with AC activated by nitric acid as a precursor and manganese nitrate as a precursor. We characterized the surface morphology, pore structure, active component phase, functional group, and active component valence change law of the Mn/AC catalyst. The denitration rate order with different Mn loadings is 7Mn/AC > 9Mn/AC > 5Mn/AC. When the Mn loading was 7%, the catalyst's surface was smooth, with a good pore structure and uniform surface distribution of metal particles. These features increased the reacting gas's contact area, improving the denitration rate. The reason for this was oxygen chemisorption on the catalyst's surface. The Mn^{4+} and the number of oxygen-containing functional groups on the catalyst surface increase after Mn loading increases; this provides more active sites for denitration and promotes the reaction's conversion to fast selective catalytic reduction. The low-temperature CO + NH₃ coupling denitration of Mn/AC catalysts conforms to the Langmuir–Hinshelwood mechanism when the temperature is lower than 230 °C and the Eley–Rideal mechanism when the temperature is higher than 230 °C. The research results can provide new ideas for low-temperature flue gas denitration.

1 Introduction

Nitrogen oxides (NO_x) are major emissions from factories and motor vehicles and are one of the most serious air pollutants.[1–3] Selective catalytic reduction (SCR) has always been an effective method for treating NO_x.[4] Carbon monoxide (CO) and ammonia (NH_3) are reducing agents for SCR. One technical advantage of CO-SCR[5,6] is that CO exists in automobile exhaust and industrial exhaust gases. Using it as a reducing agent to treat NO_x treats waste with waste; however, this method has challenges. For example, questions remain about achieving low-temperature activation and improving antioxidant capacity, *et cetera*. As the most widely used stationary source flue gas denitration method, NH_3-SCR[7] technology has many problems, including NH_3 storage, leakage, and secondary pollution. If two gases can be coupled for low-temperature denitration, on the one hand, it can use NH_3 to reduce better; on the other hand, it can use the CO existing in the exhaust gas to co-denitration, then we must overcome the drawbacks and bottlenecks inherent to separate denitration of the two gases. Therefore, it is of great significance

to explore the mechanism of CO + NH_3 coupling denitration under the condition of low-temperature flue gas.

Activated carbon (AC) is the main carrier of denitration catalysts due to its pore structure, A large number of mesoporous and microporous structures, large specific surface area, super adsorption performance, and abundant surface functional groups;[8] however, AC cannot achieve the depth of NO_x at low temperatures purification and low-temperature flue gas emission standards. Studies have shown that active metal components can be loaded into AC to improve its low-temperature denitration activities. The metals used as active components are mainly iron (Fe),[9] manganese (Mn),[10] copper (Cu),[6] cobalt (Co),[11] cerium (Ce),[10,11] platinum (Pt),[12] palladium (Pd),[13] rhodium (Rh),[14] and silver (Ag),[14,15] of which Mn has good low-temperature denitration activity.[16] In the field of NH_3-SCR denitration, J. Y. Chen *et al.*[17] found that MnO_x loaded into Fe_2O_3/AC increases amorphous dispersion, the $Fe^{3+}/(Fe^{3+} + Fe^{2+})$ and Mn^{4+}/Mn^{3+} ratio, specific surface area, and pore volume. Y. Jie *et al.*[9] found that Fe was loaded into Mn–Ce/AC, the Mn^{4+}/Mn^{n+}, Ce^{3+}/Ce^{n+} ratio, oxygen adsorbed from the surface, the number of weak and medium acid sites, and Mn valence increased. However, few studies related to CO-SCR denitration have been conducted. Consequently, the mechanism of CO denitration of the catalyst prepared by Mn loaded into carbon materials remains unclear. Hamada *et al.*[18] proposed the NH_3-SCR composite CO-SCR double-bed catalyst

aFaculty of Metallurgical and Energy Engineering, Kunming University of Science and Technology, Kunming, 650093, China. E-mail: 595762307@qq.com

bClean Metallurgy Key Laboratory of Complex Iron Resources, University of Yunnan Province, Kunming 650093, China

structure, which not only avoided the ammonia escape problem of NH_3-SCR denitration, but also made up for the narrow temperature range of CO-SCR denitration. The use of different reducing agents to stratify and step for denitration is crucial. The key of coupled denitration studied in this paper is to introduce two reducing agents at the same time to explore the reaction between them and the active component or carrier.

This article proposes loading Mn into coconut shell-AC to prepare Mn/AC series catalysts. $CO + NH_3$ serves as a composite reducing agent to denitrify low-temperature flue gas. We used scanning electron microscopy (SEM), Brunauer–Emmett–Teller (BET), Fourier-transform infrared spectroscopy (FTIR), X-ray powder diffraction (XRD), energy-dispersive X-ray spectroscopy (EDS), and X-ray photoelectron spectroscopy (XPS) to determine the surface morphology, pore structure, functional group characteristics, active component phase, and metal valence state of the Mn/AC catalyst. Then, we revealed the low-temperature $CO + NH_3$ of the Mn/AC catalyst coupling denitration mechanism. These results provide new ideas for NO_x energy-saving strategies, environmental protection management, and ultra-low emission of low-temperature flue gas.

2   Experiment

2.1   Catalyst preparation

We cleaned 200 g of coconut shell-AC with deionized water 6–7 times. The surface ash was removed, then the carbon was bathed in 60 °C water with ultrasonic vibrations for 2 h. After suction filtration, carbon was placed into a blast drying oven at 110 °C and dried for 24 h to make AC. We immersed an equal volume of 4 mol per L nitric acid solution in a three-necked flask at 80 °C with magnetic stirring and reflux for 2 h. This was subsequently placed in a drying oven at 110 °C for 24 h to obtain HNO_3/AC. We weighed three parts with a mass of 40 g HNO_3/AC with an analytical balance and took 50% $Mn(NO_3)_2$ solution as the precursor. The Mn and AC mass ratios were 5 : 100, 7 : 100, and 9 : 100, respectively. Deionized water was added

to the precursor solution, which was then immersed under ultrasonic vibration at 60 °C for 2 h. Then, the samples were suction filtered, dried at 110 °C for 24 h, and calcined at 450 °C under nitrogen protection for 4 h. The samples were recorded as 5Mn/AC, 7Mn/AC, and 9Mn/AC.

2.2   Denitration activity test

Low temperature $CO + NH_3$ coupled denitration experiments of Mn/AC catalysts were carried out in a fixed-bed reactor (Fig. 1). Before denitration, 8 g of 5Mn/AC, 7Mn/AC, and 9Mn/AC were placed in the reactor at a temperature range of 150–300 °C. The heating rate is set to 10 °C min^{-1}. When the furnace temperature reached 150 °C, simulated smoke appeared. The initial time was set as 0 min and the reaction time was 15 min, during which a data point was recorded every 3 s. Simulated flue gas setting: NO flow 4 mL min^{-1}, CO flow 16 mL min^{-1}, the NH_3 flow 4 mL min^{-1}, O_2 content 9% (volume ratio), and N_2 was the balance gas. The denitration tail gas was detected by the Testo-340 flue gas analyzer (Germany Testo Instrument Company).

$$NO \ conversion = \left(\frac{NO_{in} - NO_{out}}{NO_{in}} \right) \times 100\% \qquad (1)$$

In the formula: NO_{in} – NO concentration at the inlet of the reactor, ppm; NO_{out} – reactor outlet NO concentration, ppm.

2.3   Material characterization

We observed the microscopic morphology of the catalyst surface with an SEM (Tescan VEGAS SBH). EDS (Tescan VEGAS SBH) was used to analyze metals' local distribution and content on the catalyst's surface. The BET-BJH experiment was performed using a nitrogen adsorption–desorption tester (QDS-evo), and the specific surface area, pore volume, and average pore diameter of the catalysts were measured using an N_2 adsorption isotherm at 77 K. The supported metal oxides were analyzed by a rotating target XRD (TTR18Kw Cu target) to analyze the
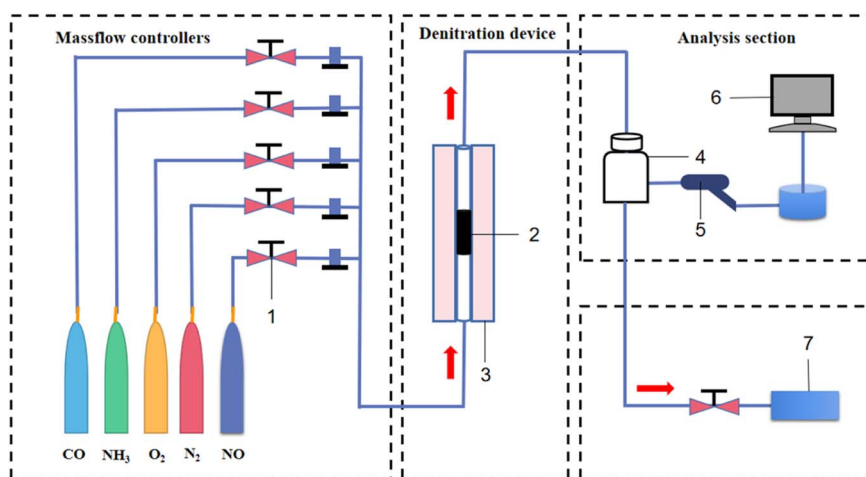

Fig. 1   Gas reaction device diagram: (1) rotameter; (2) catalyst; (3) fixed-bed reactor; (4) buffer gas cylinder; (5) detection gun; (6) flue gas analyzer; and (7) exhaust gas recovery device.

catalyst's crystal phase pattern; XPS (PHI5000 Versaprobe-II) was used to analyze the surface atomic state of the catalyst, using AlK at 50 W α X-ray ($h\nu$ = 1486.6 eV) radiation measurement, the binding energy (BE) was calibrated by using the C 1s BE value of 284.8 eV; FTIR (Nicolet iS 10), measured in the range of 4000–400 cm^{-1}.

3   Results and discussion

3.1   Low temperature CO + NH$_3$ coupled denitration activity

The CO + NH$_3$ coupling denitration activity of the Mn/AC catalyst in the range of 150–300 °C is shown in Fig. 2. The 7Mn/AC catalyst had a higher denitration rate, up to 61%, in the initial stage of the reaction. The 9Mn/AC catalyst was second to the 7Mn/AC catalyst, with a denitration rate of 55%. Meanwhile, the 5Mn/AC catalyst had the lowest denitration rate, only 36%. As Mn loading increased, the denitration rate of the catalyst increased significantly; however, when the Mn loading reached 9%, the denitration rate decreased. This might be because the pores on the catalyst's surface were blocked, and the pores collapsed,[16] weakening NO gas adsorption. When the temperature increased, the denitration rate of each catalyst gradually decreased, reaching a minimum when the temperature increased to about 230 °C. Here the denitration rate of 5Mn/AC decreased to 16.5%, the denitration rate of 7Mn/AC decreased to 32.1%, and the denitration rate of 9Mn/AC decreased to 28%. When the temperature increased further, the denitration rate of each catalyst gradually rose. The denitration rate order remained 7Mn/AC > 9Mn/AC > 5Mn/AC catalyst. For the NH$_3$-SCR reaction in the low-temperature stage, the adsorption capacity of AC was limited due to the limited metal loading capacity of the catalyst;[19] therefore, as NO gas increases, the denitration rate continues to decline. For the CO-SCR reaction, CO is adsorbed to form coordinated carbonate, and NO is adsorbed to form coordinated nitro; then, carbonate and nitro will react to generate CO and N$_2$O.[20] The denitration rate will
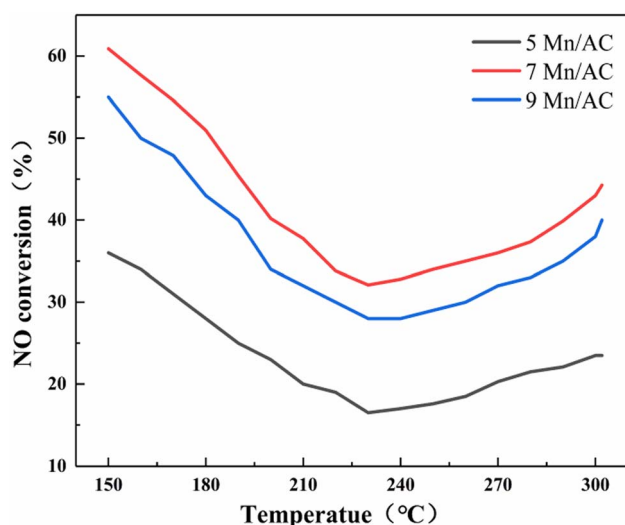
also decrease due to gradual reductions in the adsorption capacity of AC. Therefore, before the initial temperature is 230 °C, the denitration rate gradually decreases due to the reduced adsorption capacity of AC for the two separate reactions. When the temperature exceeds 230 °C, both NH$_3$-SCR and CO-SCR reactions facilitate NO conversion due to the increased temperature. Because the metal Mn is the active material of the catalyst, under its action, the lattice oxygen of AC is transformed into chemisorbed oxygen.[20] This promotes the two SCR reactions, and the denitration rate of the catalyst increases gradually after 230 °C. However, because the activated carbon is in a state of loss during the denitration process, the NO conversion rate will not rise to its initial status, even if it gradually rises.[5]

3.2   SEM and EDS

Fig. 3 shows the surface microstructure of the Mn/AC catalyst. In Fig. 3(a) and (b), the 5Mn/AC catalyst surface shows an uneven pore distribution with a small number of surrounding particles. Oxides 1, 2, and 3 in Fig. 3(b) were selected for EDS. The elemental analysis results are shown in Table 1. When the Mn loading was 5%, a small amount of Mn could be detected in the massive attachments indicated by the catalyst. This indicates that the catalyst is successfully loaded with Mn; however, its content is low.

In Fig. 3(c) and (d), the 7Mn/AC catalyst has a smooth surface, developed pore structure, significantly increased pore channels, and uniform particle distribution on the surface. This helps the catalyst adsorb gases. Oxides 4, 5, and 6 in Fig. 3(d) were selected for EDS elemental analysis (Table 1). The 7Mn/AC catalyst successfully supports the Mn element with moderate content and can modify the AC well. These findings are consistent with the results of the denitration curve in Fig. 2.

In Fig. 3(e) and (f), the 9Mn/AC catalyst has a rough surface, uneven distribution of differently sized pores, and local accumulation of particles on the surface. These factors block the pores and inhibit denitration. Oxides 7, 8, and 9 in Fig. 3(f) were selected for EDS elemental analysis; the results are shown in Table 1. When the Mn loading was 9%, massive attachments were detected on the catalyst's surface. The high Mn content indicated that excessive loading of Mn may lead to accumulation and blockage of pores on the catalyst's surface[21] (Fig. 3(e) and (f)). This may be one reason the NO conversion rate is reduced due to excessive loading.

3.3   Pore structure

The BET data of Mn/AC series catalysts are shown in Table 2. The 7Mn/AC catalyst had the largest specific surface area, 795 m^2 g^{-1}, and the 5Mn/AC and 9Mn/AC catalysts had specific surface areas of 717 m^2 g^{-1} and 728 m^2 g^{-1}, respectively. The surface area and pore structure of the catalyst affects a catalyst's denitration activity,[22] which is also consistent with the denitration activity sequence shown in Fig. 2.

Fig. 4(a) shows that the relative pressures of the adsorption–desorption curves of the Mn/AC catalysts were between 0.4 and 0.8. According to the International Union of Pure and Applied Chemistry, all samples show typical type IV adsorption. The
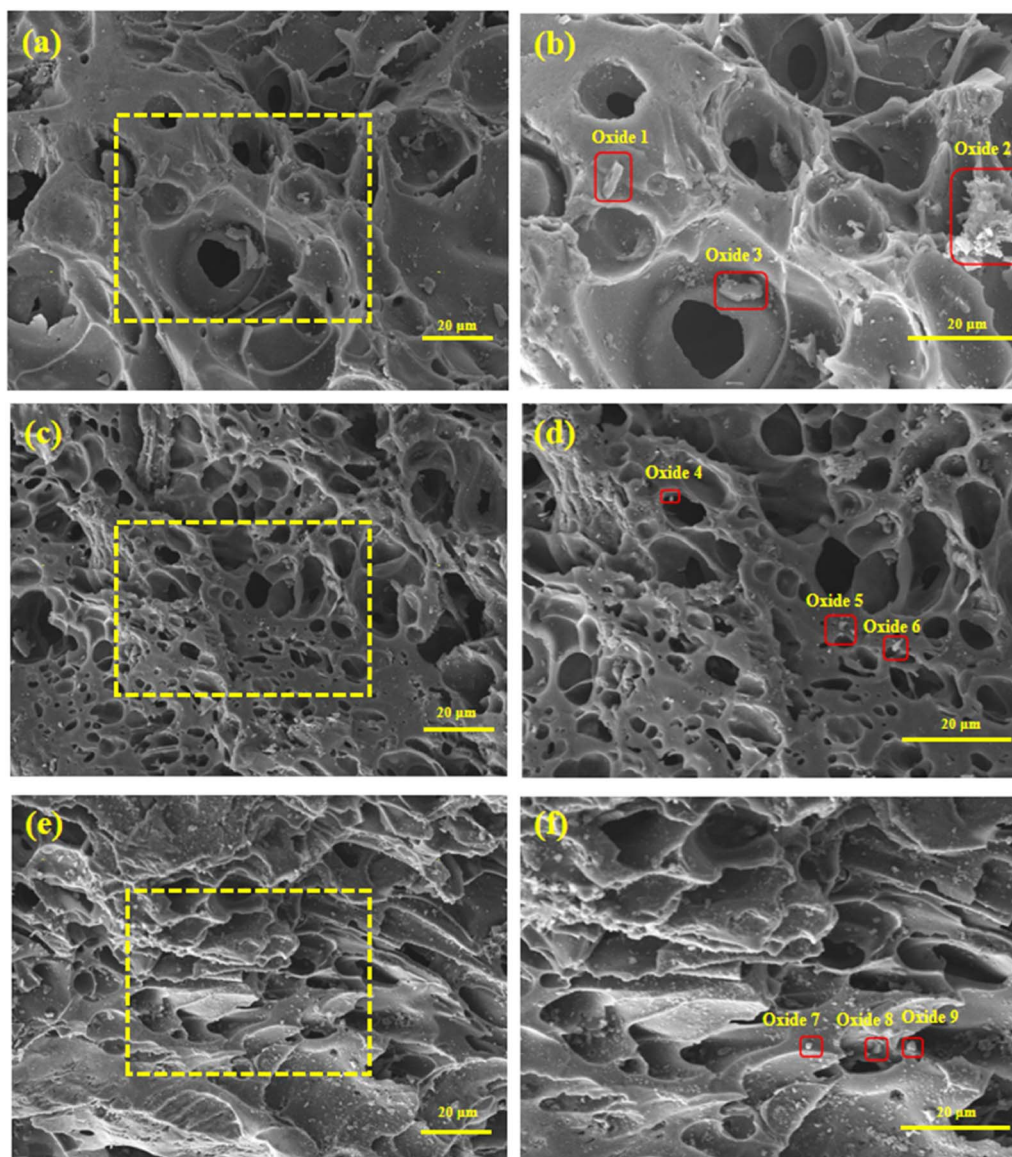

Fig. 2   NO conversion rate of the Mn/AC catalysts.

Fig. 3 SEM image of Mn/AC catalysts: (a) 5Mn/AC × 300; (b) 5Mn/AC × 500; (c) 7Mn/AC × 300; (d) 7Mn/AC × 500; (e) 9Mn/AC × 300; (f) 9Mn/AC × 500.

Table 1 EDS characterization elements and the contents of Mn/AC catalysts

Oxides	Elements (%)					
	Mn	O	C	S	Al	Si
Oxide 1	1.32	6.04	85.66	0.49	0.16	0
Oxide 2	3.31	4.35	81.96	0.55	0.24	0.18
Oxide 3	2.24	6.00	91.26	0.26	0.12	0.12
Oxide 4	12.31	7.19	78.53	0	1.46	0
Oxide 5	6.30	10.06	84.86	0.32	0	0
Oxide 6	7.01	9.90	85.45	0	0	0
Oxide 7	14.01	21.96	62.15	0.14	0.13	0.10
Oxide 8	8.67	27.20	59.44	0.15	2.86	4.69
Oxide 9	5.84	16.46	76.76	0.15	0	0.08

isotherm with an H4-type hysteresis loop[23] belongs to the slit pores. The pores are generated by the layered structure and indicate many micropores and mesopores inside the catalyst. Still, the pore structure is slightly different due to different loadings: the 5Mn/AC catalyst has fewer pores on the surface, and the pores are not developed. The 9Mn/AC catalyst's surface has more loading and local accumulation. Here, the surface

Table 2 Pore structure parameter values for Mn/AC catalysts

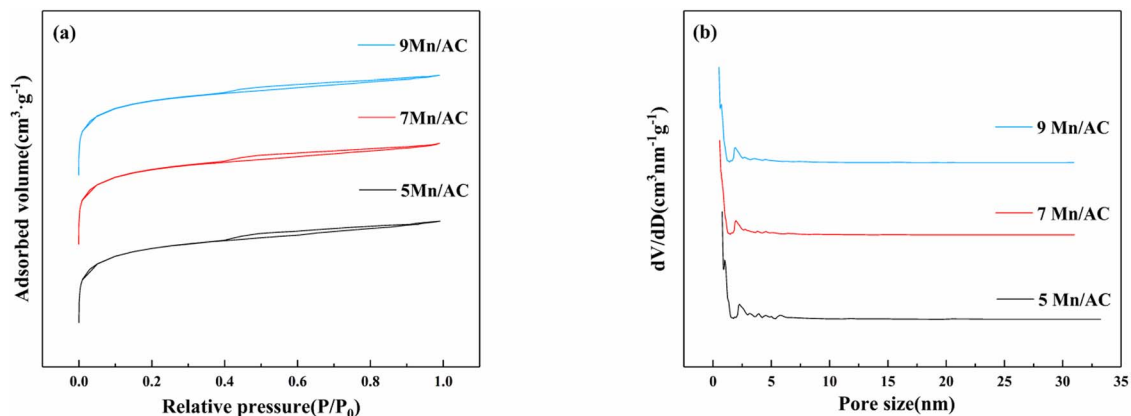| Catalysts	Surface area (m^2 g^{-1})	Total pore volume (cm^3 g^{-1})	Average pore diameter (nm)
5Mn/AC	717	0.358	2.0
7Mn/AC	795	0.399	2.0
9Mn/AC	728	0.360	2.0

Fig. 4 Pore structure characteristics: (a) N$_2$ adsorption–desorption curve and (b) average pore size distribution.

particles block the pores, and the pores collapse, as shown in Table 2. The specific surface area and average pore size of the 9Mn/AC catalyst were lower than the other two catalysts. This greatly reduces its adsorption capacity for reaction gases, thereby decreasing its denitration activity. The specific surface area and pore volume of the catalyst directly affect its mass transfer and adsorption of the reaction gas during the reaction process,[24] thereby affecting NO conversion. Fig. 4(b) depicts the average micropore size distribution for the catalyst material. The corresponding pore size distribution curve from the isotherm's adsorption branch was obtained using the BJH method. The average pore diameter of the Mn/AC catalyst was 2 nm. When the loading was too large, the supported metal collapsed the pores, reducing the contact area with the adsorbed gas. Conversely, when the loading was too small, the catalyst featured many poorly developed macropores, making the pore size large. However, the NO conversion of mesopores and micropores are optimized then that of the macropore. For catalysts, the more mesopores and micropores on the surface, the more conducive the surface is to metal loading and gas adsorption.[25,26] Therefore, 5Mn/AC has bigger pore size and lower NO conversion. This result is consistent with the SEM results (Fig. 3).

3.4 XRD analysis

Fig. 5 depicts the XRD pattern of the Mn/AC catalyst. A diffraction peak can be observed at 20–30°. This represents a graphite crystallite (002) crystal plane with a layered structure (JCPSF = 13-0148).[27] A sharp diffraction peak can be observed at 25–30°, corresponding to SiO$_2$ (JCPSF = 46-1045).[9] In addition, the diffraction peaks at 2θ of 36.4°, 38.4°, and 58.6° of the Mn/AC catalyst correspond to MnO (JCPDS = 04-0326). The diffraction peaks at 2θ of 32.9°, 55.2°, and 65.8° correspond to Mn$_2$O$_3$ (JCPDS = 41-1442). The diffraction peaks at 2θ of 36.8°, 43.5°, and 65.4° correspond to MnO$_2$ (JCPDS = 44-0141).[28] The diffraction peaks of MnO$_x$ on the surface of each catalyst are weak, indicating that the crystallinity is low. MnO$_x$ with low crystallinity increases the number of oxygen vacancies, and the active components all contain MnO, Mn$_2$O$_3$, and MnO$_2$; the EDS results are the same. The MnO$_x$ diffraction peak on the surface of the 5Mn/AC catalyst is weak, indicating that it is dispersed over the AC surface in an amorphous state. Here, the small content is consistent with the SEM results. On the surface of the 7Mn/AC catalyst, the diffraction peak of MnO is weak, indicating that it is uniformly dispersed on the catalyst's surface. This helps increase the contact area of the reaction gas and improves denitration efficiency. In contrast, the diffraction peak of MnO$_x$ of the 9Mn/AC catalyst is stronger because excessive loading of manganese oxides leads to agglomeration.[29]
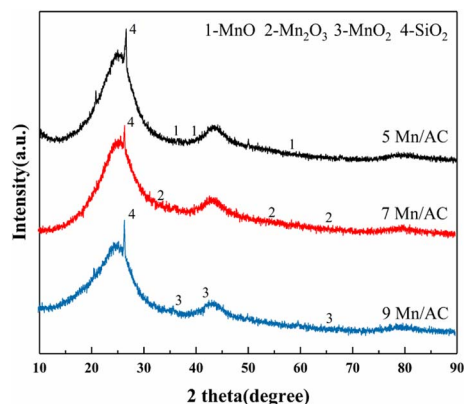
3.5 XPS analysis

The XPS characterization method studies valence states and concentrations of elements on the catalyst's surface, as shown in Table 3 and Fig. 6. Fig. 6(a) is the O 1s XPS spectrum of the

Fig. 5 XRD spectrum of Mn/AC catalysts.

Table 3 Surface atomic concentration of different catalyst samples

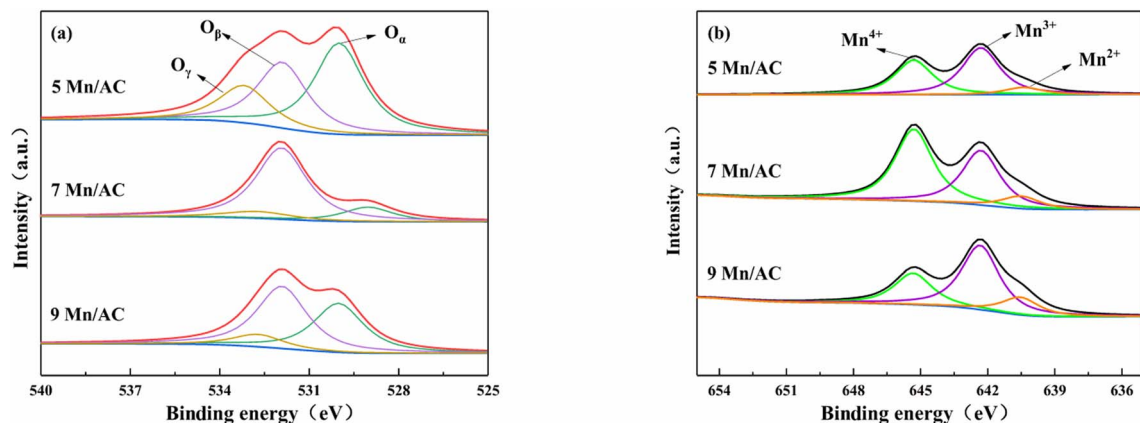| Catalysts	O$_\beta$/(O$_\alpha$ + O$_\beta$ + O$_\gamma$)%	Mn^{4+}/(Mn^{2+} + Mn^{3+} + Mn^{4+})%	Mn^{3+}/(Mn^{2+} + Mn^{3+} + Mn^{4+})%
5Mn/AC	33.907	38.983	33.876
7Mn/AC	76.257	51.771	45.762
9Mn/AC	73.563	27.790	36.560

Fig. 6 XPS characterization of Mn/AC catalysts: (a) O 1s and (b) Mn 2p.

Mn/AC catalyst. The fitted peaks in the figure can be divided into three types: lattice oxygen O_α (529.0–530.0 eV), chemisorbed oxygen O_β (531.3–531.9 eV), and hydroxyl oxygen O_γ (532.7–533.5 eV).[30,31] As presented in Table 3 and Fig. 6, the order of chemically adsorbed oxygen content is 7Mn/AC > 9Mn/AC > 5Mn/AC. With the loading increase, the redox reaction between Mn^{4+} and Mn^{3+} forms more reactive oxygen vacancies, which increases the O_β content. In addition, O_β contributes to NO oxidation to NO_2, promoting the standard SCR reaction to the fast SCR reaction.[26] However, agglomeration occurs on the catalyst's surface when the loading is too large. This can block the pores and occupy oxygen vacancies, reducing NO's conversion rate. These results are also consistent with the SEM results.

Fig. 6(b) is the Mn 2p XPS spectrum of the Mn/AC catalyst. The three diffraction peaks correspond to Mn^{2+} (640.4–640.5 eV), Mn^{3+} (642.3–644.8 eV) and Mn^{4+} (645.3–645.9 eV) of Mn 2p respectively.[30,32] Manganese oxides with different valence states also affect the SCR reaction differently. In the graph, the 7Mn/AC catalyst had more Mn^{4+} than 5Mn/AC. The Mn^{4+} content in the 9Mn/AC catalyst was the lowest. With the increase of Mn loading, the characteristic peaks of Mn^{4+} and Mn^{3+} are continuously enhanced, while the characteristic peaks of Mn^{2+} are weakened, indicating that the average valence state of Mn ions on the surface of 7Mn/AC catalyst is higher, and the contents of Mn^{4+} and Mn^{3+} ions are also increasing. However, after excessive loading, Mn oxides aggregate on the surface of the catalyst, resulting in the reduction of active components. Studies[31] have shown that Mn^{4+} had high N_2 selectivity in the SCR reaction and demonstrated that Mn^{4+} exhibited higher N_2 selectivity than Mn^{3+} and Mn^{2+} in the catalytic degradation of NO and N_2O, and more Mn^{4+} promotes NO oxidation to NO_2, thereby promoting the SCR reaction to the fast SCR reaction ($NO + NO_2 + 2NH_3 \rightarrow 2N_2 + 3H_2O$). Mn^{3+} is preferentially reduced to Mn^{2+} in the reduction stage. The coexistence of Mn^{4+} and Mn^{3+} can promote the catalytic activity of the catalyst. The higher the content, the stronger the redox and the more oxygen vacancies are generated, thereby improving the denitration efficiency. The presence of more Mn^{4+} on the catalyst's surface helps improve the denitration efficiency at low temperatures; consequently, the 7Mn/AC catalyst has the highest NO conversion rate.

3.6 FTIR analysis

Fig. 7 depicts the FTIR spectrum of the Mn/AC catalyst. The infrared peaks at 3414 cm^{-1} are considered the stretching vibration peaks of carboxyl and OH functional groups;[33] the infrared peaks at 1621 cm^{-1} are C=O stretching vibration peaks on aliphatic groups;[27] at 1390 cm^{-1}, the absorption peaks of cycloalkanes and aliphatic hydrocarbons are C–H stretching vibration peaks;[28] the absorption peaks at 1128 cm^{-1} are the stretching vibration peaks of C–O in C–O–C bonds such as lactones, phenols, and ethers, functional groups on the surface of AC.[30] Fig. 7 shows that the functional groups of Mn/AC catalysts with different Mn loadings are basically the same.

The area order of the stretching vibration absorption peaks of –COOH in the vicinity of 3414 cm^{-1} and –OH in chemically adsorbed water for each catalyst is 7Mn/AC > 9Mn/AC > 5Mn/AC. This indicates that when the Mn loading is too low, there are fewer functional groups. This is not conducive to denitration. Agglomeration of the catalyst surface destroys the carboxyl and the O–H functional groups in the chemically adsorbed water.[31] The asymmetric vibration absorption peak of the 7Mn/AC catalyst at 1618 cm^{-1} is compared with the other two catalysts. Obviously, there are more C=O groups. Many oxygen vacancies or active sites have developed in the catalyst. Studies have reported that NO adsorption occurs in the C=O
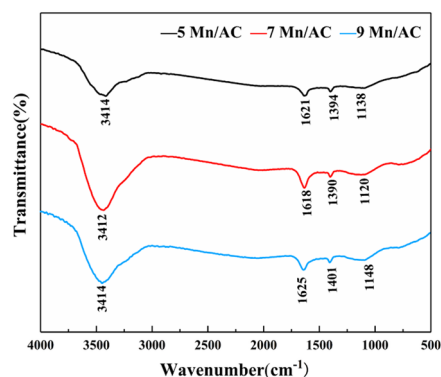

Fig. 7 FTIR spectrum of Mn/AC catalysts.

part. The surface oxygen-containing functional groups improve the dispersion of active components, forming an adsorption site for CO.[26] Peaks at 1120, 1138, and 1148 cm^{-1} correspond to carbonyl, carboxyl, phenolic C–OH stretching vibration, and ether-based C–O stretching vibration absorption peaks. As seen in Fig. 7, the C–O stretching vibration absorption peak increased as the Mn loading ratio increased. This may be because the doping of metal Mn increased the number of oxygen-containing functional groups on the catalyst's surface. In summary, the surface of the 7Mn/AC catalyst has many adsorption sites, such as carboxyl groups and lactone groups. The increase of oxygen-containing functional groups provides more active sites for denitration and can facilitate the first stage of denitration. More O_β promotes the SCR reaction.

3.7 CO + NH₃ coupling low-temperature denitration mechanism

Based on the above results, we propose that Mn/AC series catalysts coupled with the low-temperature denitration reaction process.

(1) CO, NH₃, and NO are continuously diffused from the outside of the Mn/AC catalyst to the inner surface. The reactive gases are adsorbed on the surface of the catalyst in an adsorbed state on the active site and then activated by the active site to form an adsorbed state (eqn (2)–(4)).

(2) Adsorbed CO and NO follow the Langmuir–Hinshelwood (L–H) mechanism to generate CO₂ and N₂ (eqn (5)).[5] The low-temperature SCR denitration reaction of NH₃ over carbon-based catalysts follows the Eley–Rideal (E–R) and L–H mechanisms. One study showed[16] that it mainly followed the L–H mechanism at low temperatures (150–230 °C). After the first stage of gas adsorption, ammonium ions NH^{4+} are formed; then, the adsorbed ammonium ions decompose into amino groups, two hydrogen ions, and one electron (eqn (6)). Above 230 °C, the E–R mechanism dictates that adsorbed NH₃ reacts with oxygen to form amino compounds and hydroxides (OH$^-$) (eqn (7)). Due to the different mechanisms followed by NH₃-SCR at 230 °C, there is a turning point in the denitration efficiency at

this node. The NO conversion rate corresponding to Fig. 2 also has a turning point change at 230 °C.[5]

(3) During the catalytic denitration process of active metal components,[30] a small amount of Mn^{2+} is oxidized to Mn^{3+} by the adsorbed NO. NO itself is reduced to N₂O (eqn (8)). High valence Mn^{3+} is first reduced to Mn₃O₄ and then reduced to Mn^{2+} (eqn (9)). For high valence Mn^{4+}, it is first reduced to Mn^{3+} and then reduced to Mn^{2+} (eqn (10)). During recombination and denitration of active substances, the adsorbed NO is oxidized by Mn^{4+} to NO^{2-}. NO^{2-} reacts with the adsorbed NH₃ to generate N₂ and H₂O (eqn (11)), while the adsorbed CO reacts with O_β on the catalyst's surface and with O_α and free O_α to generate CO₂ (eqn (12)). The adsorbed NO will also dissociate under the action of the catalyst, yielding N₂ and O (eqn (13)). Therefore, in the Mn/AC catalyst, the higher the Mn^{4+} content, the more effective the NO conversion. The results of this study are consistent with the XPS results.

(4) Finally, the gases (CO₂, N₂, and H₂O) generated from the catalyst's surface are desorbed and diffused to the inner surface through the AC pores.[9] Then, the gases diffuse from the AC inner surface to the outer surface of the Mn/AC catalyst (eqn (14)–(16)).
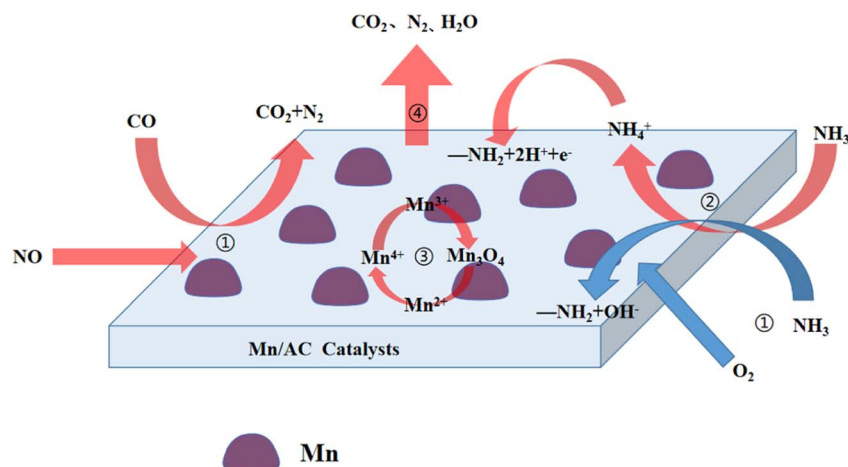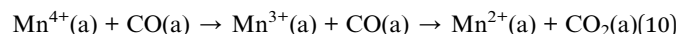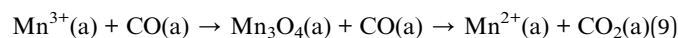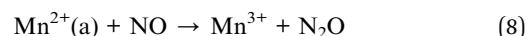
$$CO(g) \rightarrow CO(a) \tag{2}$$

$$NH_3(g) \rightarrow NH_3(a) \tag{3}$$

$$NO(g) \rightarrow NO(a) \tag{4}$$

$$CO(a) + NO(a) \rightarrow CO_2(a) + N_2(a) \tag{5}$$

$$NH_3(a) \rightarrow NH_4^+(a) \rightarrow NH_2 + 2H^+ + e^- \tag{6}$$

$$NH_3(a) + O_2(a) \rightarrow NH_2 + OH^- \tag{7}$$

$$Mn^{2+}(a) + NO \rightarrow Mn^{3+} + N_2O \tag{8}$$

$$Mn^{3+}(a) + CO(a) \rightarrow Mn_3O_4(a) + CO(a) \rightarrow Mn^{2+}(a) + CO_2(a) \tag{9}$$

$$Mn^{4+}(a) + CO(a) \rightarrow Mn^{3+}(a) + CO(a) \rightarrow Mn^{2+}(a) + CO_2(a) \tag{10}$$
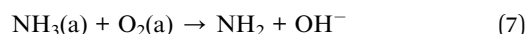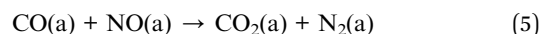

Fig. 8 Mechanism of low-temperature CO + NH₃ coupling denitration diagram of Mn/AC catalysts.

$$NO(a) + Mn^{4+}(a) \rightarrow Mn^{3+}(a) + NO_2^-(a) + NH_3(a) \rightarrow N_2(a) + H_2O(a) \tag{11}$$

$$CO(a) + O_2(a) \rightarrow CO_2(a) \tag{12}$$

$$2NO(a) \rightarrow N_2(a) + 2O(a) \tag{13}$$

$$CO_2(a) \rightarrow CO_2(g) \tag{14}$$

$$N_2(a) \rightarrow N_2(g) \tag{15}$$

$$H_2O(a) \rightarrow H_2O(g) \tag{16}$$
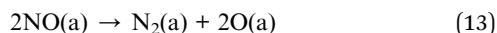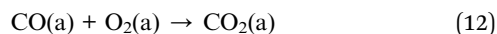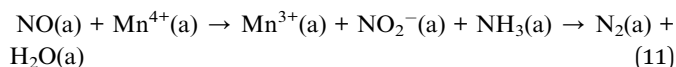
According to the above reaction process, the mechanism diagram of low-temperature $CO + NH_3$ coupling denitration of Mn/AC catalyst is proposed (Fig. 8).

4 Conclusions

This study prepared Mn/AC series catalysts and studied their low-temperature coupled denitration activity in the $CO + NH_3$ atmosphere. The denitration efficiency of the 7Mn/AC catalyst, with Mn loading of 7%, was the best and reached 61%. SEM and BET characterizations showed that the 7Mn/AC catalyst has a well-developed pore structure, a large specific surface area, and widely dispersed supports. Combined with EDS and XRD characterization, MnO on the surface of the 7Mn/AC catalyst was amorphous. The XPS characterization shows that high O_β and Mn^{4+} on the surface of the 7Mn/AC catalyst convert the standard SCR reaction to the fast SCR reaction, promoting the denitration reaction. FTIR characterization found that the content of functional groups on the surface of the 7Mn/AC catalyst was more than that of the other two catalysts. This improved NO adsorption and improved the denitration efficiency. Based on the characterization results of physical and chemical properties, a low-temperature $CO + NH_3$ denitration mechanism of Mn/AC catalyst is proposed.

The low-temperature $CO + NH_3$ coupling denitration of the Mn/AC catalyst conforms to the L–H mechanism when the temperature is lower than 230 °C and the E–R mechanism when the temperature is higher than 230 °C. Higher Mn^{4+} content promotes NO oxidation to NO_2, thereby promoting the SCR reaction to the fast SCR reaction.

Conflicts of interest

There are no conflicts to declare.

References

1 L. Yao, Q. C. Liu, S. Mossin, D. Nielsen, M. Kong, L. J. Jiang, J. Yang, S. Ren and J. Wen, Promotional effects of nitrogen doping on catalytic performance over manganese-containing semi-coke catalysts for the NH_3-SCR at low temperatures, *J. Hazard. Mater.*, 2020, **387**, 121704.

2 L. J. Jiang, X. Y. Jiang, W. Z. Liu, H. L. Wu, G. Hu, J. Yang, J. Cao, Y. Liu and Q. C. Liu, Comparative study on the physicochemical properties and de-NO_x performance of waste bamboo-derived low-temperature NH_3-SCR catalysts, *Res. Chem. Intermed.*, 2021, **47**(12), 5303–5320.

3 L. J. Jiang, Y. Liang, W. Z. Liu, H. L. Wu, T. Aldahri, D. S. Carrero and Q. C. Liu, Synergistic effect and mechanism of FeO_x and CeO_x co-doping on the superior catalytic performance and SO_2 tolerance of Mn-Fe-Ce/ACN catalyst in low-temperature NH_3-SCR of NO_x, *J. Environ. Chem. Eng.*, 2021, **9**(6), 106360.

4 G. Li, D. S. Mao, M. X. Chao, G. H. Li, J. Yu and X. M. Guo, Low-temperature NH_3-SCR of NO_x over $MnCeO_x/TiO_2$ catalyst: Enhanced activity and SO_2 tolerance by modifying TiO_2 with Al_2O_3, *J. Rare Earths*, 2021, **39**(7), 805–816.

5 B. F. Huang, Z. Shi, Z. Y. Yang, M. Dai, Z. J. Wen, W. J. Li, G. Y. Zi and L. B. Luo, Mechanism of CO selective catalytic reduction denitration on Fe-Mn/AC catalysts at medium and low temperatures under oxygen atmosphere, *Chem. Eng. J.*, 2022, **446**, 137412.

6 D. F. Wang, B. F. Huang, Z. Shi, H. M. Long, L. Li, Z. Y. Yang and M. Dai, Cu-Ni/AC Catalyst for Low-Temperature CO-Selective Catalytic Denitration Mechanism, *Ind. Eng. Chem. Res.*, 2021, **60**(43), 15443–15453.

7 L. Chen, S. Ren, W. Z. Liu, J. Yang, Z. C. Chen, M. M. Wang and Q. C. Liu, Low-temperature NH3-SCR activity of M (M = Zr, Ni and Co) doped MnO_x supported biochar catalysts, *J. Environ. Chem. Eng.*, 2021, **9**(6), 15443–15453.

8 Y. H. Zhou, B. X. Su, S. Ren, Z. C. Chen, Z. H. Su, J. Yang, L. Chen and M. M. Wang, Nb_2O_5-modified Mn-Ce/AC catalyst with high $ZnCl_2$ and SO_2 tolerance for low-temperature NH_3-SCR of NO, *J. Environ. Chem. Eng.*, 2021, **9**(5), 106323.

9 J. Yang, S. Ren, T. S. Zhang, Z. H. Su, H. M. Long, M. Kong and L. Yao, Iron doped effects on active sites formation over activated carbon supported Mn-Ce oxide catalysts for low-temperature SCR of NO, *Chem. Eng. J.*, 2020, **379**, 122398.

10 M. M. Wang, B. X. Su, S. Ren, W. Z. Liu, J. Yang, Z. C. Chen and L. Chen, Different lead species deactivation on Mn-Ce activated carbon supported catalyst for low-temperature SCR of NO with NH_3: Comparison of $PbCl_2$, Pb $(NO_3)_2$ and $PbSO_4$, *J. Colloid Interface Sci.*, 2022, **622**, 549–561.

11 J. Chen, B. Zhu, T. Du, Y. Sun, Z. Zhu, S. Yin and D. Zhang, Low-temperature Selective Catalytic Reduction of NO_x with NH_3 over Co Modified Fe_2O_3/AC Catalysts, *Nonferrous Met. Eng.*, 2017, **7**(2), 99–102.

12 Y. Inomata, M. Mino, S. Hata, E. Kiyonaga, K. Morita, K. Hikino, K. Yoshida, M. Haruta and T. Murayama, Low-temperature NH_3-SCR Activity of Nanoparticulate Gold Supported on a Metal Oxide, *J. Jpn. Pet. Inst.*, 2019, **62**(5), 234–243.

13 L. P. Sheng, S. D. Li, Z. X. Ma, F. Wang, H. He, Y. Gao, B. Zhu, Y. Wang and H. S. Yang, Mechanistic insight into the influence of O_2 on N_2O formation in the selective catalytic reduction of NO with NH_3 over Pd/CeO_2 catalyst, *Catal. Sci. Technol.*, 2021, **11**(5), 1709–1716.

14 J. Q. Xu, T. Tang, Q. Zhang, C. Zhang and F. Guo, Remarkable low temperature catalytic activity for SCR of NO with propylene under oxygen-rich conditions over

$Mn_{0.2}La_{0.07}Ce_{0.05}O_x$/ZSM-5 catalyst, *Vacuum*, 2021, **188**, 110174.

15 W. J. Liu, Y. F. Long, Y. Y. Zhou, S. N. Liu, X. Tong, Y. J. Yin, X. Y. Li, K. Hu and J. J. Hu, Excellent low temperature NH_3-SCR and NH_3-SCO performance over Ag-Mn/Ce-Ti catalyst: Evaluation and characterization, *Mol. Catal.*, 2022, **528**, 112510.

16 Z. H. Su, S. Ren, Z. C. Chen, J. Yang, Y. H. Zhou, L. J. Jiang and C. Yang, Deactivation Effect of CaO on Mn-Ce/AC Catalyst for SCR of NO with NH_3 at Low Temperature, *Catalysts*, 2020, **10**(8), 2073–4344.

17 J. Y. Chen, B. Z. Zhu, Y. L. Sun, S. L. Yin, Z. C. Zhu and J. X. Li, Investigation of Low-Temperature Selective Catalytic Reduction of NO_x with Ammonia over Mn-Modified Fe_2O_3/AC Catalysts, *J. Braz. Chem. Soc.*, 2018, **29**(1), 79–87.

18 H. Hamada and M. Haneda, A review of selective catalytic reduction of nitrogen oxides with hydrogen and carbon monoxide, *Appl. Catal., A*, 2012, **421**, 1–13.

19 L. G. Wei, R. T. Guo, J. Zhou, B. Qin, X. Chen, Z. X. Bi and W. G. Pan, Chemical deactivation and resistance of Mn-based SCR catalysts for NO_x removal from stationary sources, *Fuel*, 2022, **316**, 123438.

20 L. Y. Wang, X. X. Cheng, Z. Q. Wang, C. Y. Ma and Y. K. Qin, Investigation on Fe-Co binary metal oxides supported on activated semi-coke for NO reduction by CO, *Appl. Catal., B*, 2017, **201**, 636–651.

21 S. M. Liu, R. T. Guo, P. Sun, S. X. Wang, W. G. Pan, M. Y. Li, S. W. Liu, X. Sun and J. Liu, The enhancement of Zn resistance of Mn/TiO_2 catalyst for NH_3-SCR reaction by the modification with $Al_2(SO_4)_3$, *J. Taiwan Inst. Chem. Eng.*, 2017, **78**, 370–377.

22 S. L. Yin, B. Z. Zhu, Y. L. Sun, Z. H. Zi, Q. L. Fang, G. B. Li, C. Chen, T. Y. Xu and J. X. Li, Effect of Mn addition on the low-temperature NH_3-selective catalytic reduction of NO_x over Fe_2O_3/activated coke catalysts: Experiment and mechanism, *Asia-Pac. J. Chem. Eng.*, 2018, **13**(5), e2231.

23 L. J. Jiang, Q. C. Liu, Q. Zhao, S. Ren, M. Kong, L. Yao and F. Meng, Promotional effect of Ce on the SCR of NO with NH_3 at low temperature over MnO_x supported by nitric acid-modified activated carbon, *Res. Chem. Intermed.*, 2018, **44**(3), 1729–1744.

24 C. Z. Sun, Y. J. Tang, F. Gao, J. F. Sun, K. L. Ma, C. J. Tang and L. Dong, Effects of different manganese precursors as promoters on catalytic performance of $CuO-MnOx/TiO_2$ catalysts for NO removal by CO, *Phys. Chem. Chem. Phys.*, 2015, **17**(24), 15996–16006.

25 F. D. Liu, Y. B. Yu and H. He, Environmentally-benign catalysts for the selective catalytic reduction of NO_x from diesel engines: structure-activity relationship and reaction mechanism aspects, *Chem. Commun.*, 2014, **50**(62), 8445–8463.

26 Y. Zheng, Y. Y. Guo, X. F. Xu and T. Y. Zhu, Study of Cu/Mn Catalysts for Coreactions of NH_3-SCR and CO Oxidation, *Catal. Lett.*, 2022, **152**(6), 1752–1759.

27 A. Sharma, R. K. Dutta, A. Roychowdhury, D. Das, A. Goyal and A. Kapoor, Cobalt doped CuO nanoparticles as a highly efficient heterogeneous catalyst for reduction of 4-nitrophenol to 4-aminophenol, *Appl. Catal., A*, 2017, **543**, 257–265.

28 L. P. Liu, X. D. Wu, Y. Ma, X. Zhang, R. Ran, Z. C. Si and D. Weng, Potassium deactivation of Cu-SSZ-13 catalyst for NH_3-SCR: Evolution of salts, zeolite and copper species, *Chem. Eng. J.*, 2020, **383**, 123080.

29 J. Yang, S. Ren, B. X. Su, M. M. Wang, L. Chen and Q. C. Liu, Understanding the dual-acting of iron and sulfur dioxide over Mn-Fe/AC catalysts for low-temperature SCR of NO, *Mol. Catal.*, 2022, **519**, 112150.

30 J. Pasel, P. Kassner, B. Montanari, M. Gazzano, A. Vaccari, W. Makowski, T. Lojewski, R. Dziembaj and H. Papp, Transition metal oxides supported on active carbons as low temperature catalysts for the selective catalytic reduction (SCR) of NO with NH_3, *Appl. Catal., B*, 1998, **18**(3–4), 199–213.

31 T. Boningari, P. R. Ettireddy, A. Somogyvari, Y. Liu, A. Vorontsov, C. A. McDonald and P. G. Smirniotis, Influence of elevated surface texture hydrated titania on Ce-doped Mn/TiO_2 catalysts for the low-temperature SCR of NOx under oxygen-rich conditions, *J. Catal.*, 2015, **325**, 145–155.

32 L. A. Sun, Y. J. Xu, Q. Q. Cao, B. Q. Hu, C. Wang and G. H. Jing, Reactions and Mechanisms of Low-Temperature Selective Catalytic Reduction of NO_x by NH_3 over Manganese Oxide-Based Catalysts, *Prog. Chem.*, 2010, **22**(10), 1882–1891.

33 W. T. Yao, S. H. Yu, Y. Zhou, J. Jiang, Q. S. Wu, L. Zhang and J. Jiang, Formation of uniform CuO nanorods by spontaneous aggregation: Selective synthesis of CuO, Cu_2O, and Cu nanoparticles by a solid-liquid phase arc discharge process, *J. Phys. Chem. B*, 2005, **109**(29), 14011–14016.